

# Shallow Faults Reactivated by Hydraulic Fracturing: The 2019 Weiyuan Earthquake Sequences in Sichuan, China

Maomao Wang<sup>\*1</sup>, Hongfeng Yang<sup>2</sup>, Lihua Fang<sup>3</sup>, Libo Han<sup>3</sup>, Dong Jia<sup>4</sup>, Danqi Jiang<sup>1</sup>, and Bing Yan<sup>1</sup>

## Abstract

Human activity-induced earthquakes are emerging as a global issue, and revealing its underlying mechanisms is essential for earthquake hazard mitigation and energy development. We investigated the relationship between the seismotectonic model and seismic sequences from moderate  $M_w$  4.3 and  $M_w$  5.2 earthquakes that occurred in February and September 2019, respectively, in the Weiyuan anticline of Sichuan basin, China. We found that the  $M_w$  5.2 earthquake ruptured a back thrust of structural wedges and released most aftershocks near the wedge tip. However, the two foreshocks of the  $M_w$  4.3 earthquake sequence occurred in hydrofractured Silurian shale at depth of 2.5–3 km, and the mainshock ruptured the overlying oblique tear fault at a depth of  $\sim 1$  km. Hydraulic fracturing in the sedimentary cover of this block may induce earthquakes through fluid pressure diffusion in the Silurian shale and through poroelastic effects on back thrusts within structural wedges, respectively. We assessed the hazard potential of four seismic sources in the Weiyuan block and suggest it is critical to conduct a coupled flow-geomechanics assessment and management on induced seismicity and related cascading effects in the densely inhabited and seismically active Sichuan basin.

**Cite this article as** Wang, M., H. Yang, L. Fang, L. Han, D. Jia, D. Jiang, and B. Yan (2020). Shallow Faults Reactivated by Hydraulic Fracturing: The 2019 Weiyuan Earthquake Sequences in Sichuan, China, *Seismol. Res. Lett.* **XX**, 1–11, doi: [10.1785/SRL20200174](https://doi.org/10.1785/SRL20200174).

[Supplemental Material](#)

## Introduction

The injection and extraction of fluids to and from deep wells by human activities can induce seismic activity, as widely reported in North America, Europe, and East Asia (Frohlich, 2012; Ellsworth, 2013; Yang *et al.*, 2017; Grigoli *et al.*, 2018; Kim *et al.*, 2018). In general, earthquakes thought to be triggered by fluid injection are mainly attributed to two mechanisms: (1) direct fluid pressure effect of the injection, or (2) changes in solid stresses due to fluid extraction or injection (Ellsworth, 2013). The first mechanism involves weakening the pre-existing fault zone through elevated fluid pressures (Zhang *et al.*, 2013), whereas the second mechanism involves changing the loading conditions on a fault plane without direct hydrologic connection (Segall and Lu, 2015; Galloway *et al.*, 2018; Goebel and Brodsky, 2018; Jiang *et al.*, 2020). Recent studies suggest that injection-induced slow-slip events (Eyre *et al.*, 2019) and earthquake triggering effects need to be considered (H. Yang *et al.*, unpublished manuscript, 2020, see [Data and Resources](#); Yang *et al.*, 2020). With the development of shale gas, that requires the technique of horizontal wells and hydraulic fracturing (HF) (fracking), there have been reports of moderate earthquakes induced by fracking in Canada, U.S., and China (Holland, 2013; Lei *et al.*, 2017, 2019; Schultz *et al.*, 2017; Skoumal *et al.*, 2018; Wang *et al.*, 2018; Eyre *et al.*, 2019; Schultz and

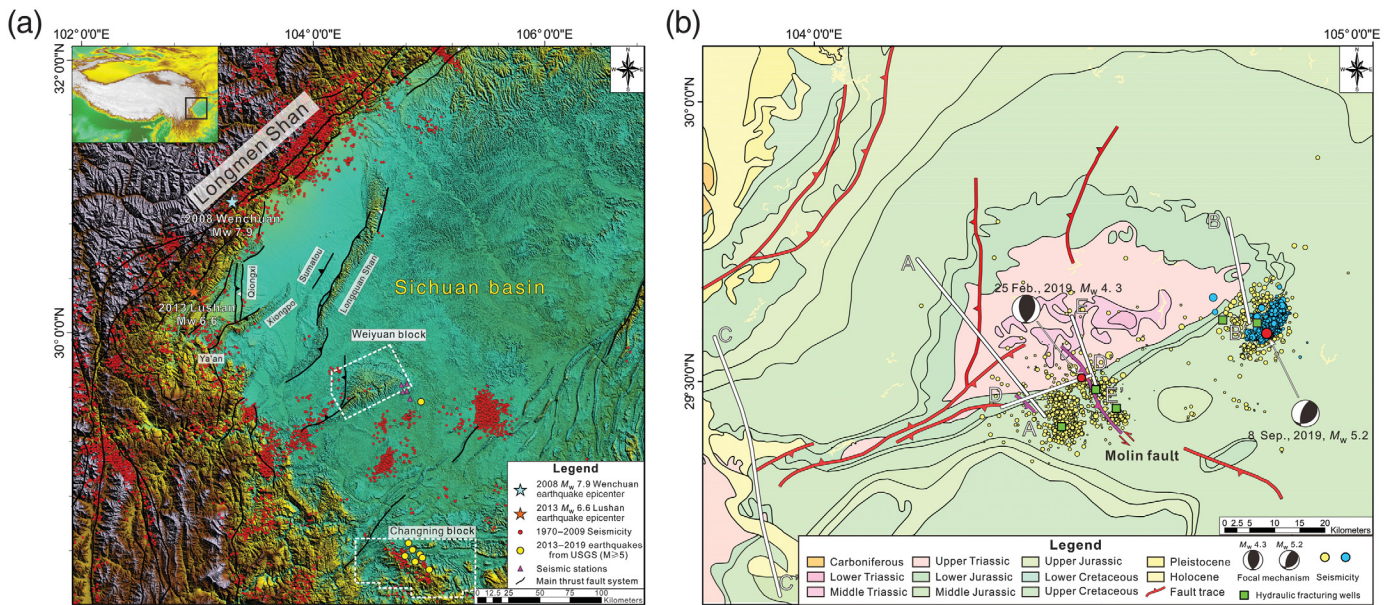
Wang, 2020; H. Yang *et al.*, unpublished manuscript, 2020, see [Data and Resources](#); Yang *et al.*, 2020). High-quality geophysical and geological data are generally available for shale gas blocks, so that excellent constraints on subsurface stratigraphy horizons, fault structures, and basement faults can be obtained in these regions. These data are critical to understanding the mechanisms of induced earthquakes and are also necessary parameters to build a reliable geomechanical model to quantitatively assess relevant hazards (Juanes *et al.*, 2016; Galis *et al.*, 2017).

Since 2010, China has conducted extensive shale gas exploration and production activities in the Sichuan basin (Fig. 1). The Silurian Longmaxi Formation shales in the Sichuan basin are the major target for shale gas HF operations (Zhai *et al.*, 2018). Unlike the tectonically stable Marcellus shale in the northeastern U.S., seismically active faults occur widely throughout the southwestern Sichuan basin (Fig. 1). From 2013 to 2019, eight earthquakes greater than  $M_w$  5 have

1. College of Oceanography, Hohai University, Nanjing, Jiangsu, China; 2. Earth System Science Programme, The Chinese University of Hong Kong, Shatin, Hong Kong, China; 3. Institute of Geophysics, China Earthquake Administration, Beijing, China; 4. Department of Earth Sciences, Nanjing University, Nanjing, China

\*Corresponding author: wangmm@hhu.edu.cn

© Seismological Society of America



occurred in the shale gas blocks of Sichuan basin, with the maximum magnitude being  $M_w$  5.8 (Table 1). Among them, 88% of the earthquake events occurred in the Changning block on the southern border of the Sichuan basin, whereas only one earthquake event occurred in the Weiyuan block (Fig. 1) (U.S. Geological Survey [USGS] Earthquake Center, 2020). On 25 February and 8 September 2019, two moderate earthquakes with moment magnitudes of  $M_w$  4.3 and 5.2 struck Rong County and Weiyuan County, respectively, in Sichuan Province (Fig. 1). These two counties are located near the Weiyuan anticline in the southern Sichuan basin, one of China's longest-producing shale gas blocks (Fig. 1). In this seismically affected area, 4 people were killed and 75 were injured. The economic loss due to the 2019 earthquakes in the Weiyuan block was estimated to be ~10 million U.S. dollars.

The February  $M_w$  4.3 earthquake was preceded by two  $M_w > 4$  foreshocks, which were suggested to occur on different faults than the mainshock according to an analysis of seismic and geodetic data (H. Yang *et al.*, unpublished manuscript, 2020, see [Data and Resources](#); Yang *et al.*, 2020). Furthermore, no surficial faults had been mapped near the epicenter of the  $M_w$  5.2 earthquake; therefore, the faults on which they occurred and the mechanisms responsible for the earthquakes are unknown. In this study, we utilized seismic reflection profiles, relocated seismicity, and focal mechanisms to analyze the seismotectonic models of the 2019  $M_w$  4.3 and  $M_w$  5.2 earthquake sequences that occurred in the Weiyuan anticline and determined the structural geometries and kinematical models of their coseismic fault structures. Furthermore, we analyzed the spatiotemporal distribution of earthquakes relative to the fault system to explore their potential relationships to HF. Finally, we quantitatively assessed the relationship between the earthquake hazard potential and fault system reactivation in this shale gas block.

**Figure 1.** (a) Topography map of the Longmen Shan and Sichuan basin. Instrumental seismicity record from 1970 to 2009 is shown in red circles. Possible induced earthquakes greater than  $M_w$  5 from 2013 to 2019 are shown in yellow circles. The inset shows the regional-scale setting of the Sichuan basin. (b) Geologic map of the Weiyuan anticline in the Sichuan basin. Northeast-trending fault traces parallel to the fold axis of the anticline are shown in red. The tear faults Ft1 and Ft2 are shown in magenta with the seismicity of the 2019 Weiyuan earthquakes. Seismic reflection profiles AA', BB', CC', DD', and EE' are illustrated as white lines.

## Geological Setting

The 2019  $M_w$  4.3 and  $M_w$  5.2 earthquake sequences occurred near the Weiyuan anticline in the southern Sichuan basin. This area is located ~200 km west of the range front of the Longmen Shan fold-and-thrust belt that produced the 2008  $M_w$  7.9 Wenchuan earthquake and the 2013  $M_w$  6.6 Lushan earthquake (Burchfiel *et al.*, 2008; Wei *et al.*, 2008; Hubbard and Shaw, 2009; Xu *et al.*, 2009; Wang *et al.*, 2014) (Fig. 1). Two-level detachment faults have formed in the Longmen Shan fold-and-thrust belt, corresponding to a 4–5 km depth Triassic evaporite detachment and a 16–18 km Precambrian basal detachment that extends from the hinterland to the Weiyuan anticline, located in the interior of the Sichuan basin (Hubbard and Shaw, 2009; Hubbard *et al.*, 2010; Jia *et al.*, 2010; Li *et al.*, 2014). In late Cenozoic, geologic slip propagated along the shallow detachment into the foreland basin and formed northeast-striking contractional thrust-related anticlines, including the 200 km long Longquan anticline (Jia *et al.*, 2006; Wang *et al.*, 2014; Wang and Lin, 2017) (Fig. 1). In the southwestern Sichuan basin, the gently dipping (~1.5°) basal detachment fault propagated far east into the foreland basin, forming a series of northeast-trending thrust ramps above the detachment fault surface (Hubbard *et al.*, 2010).

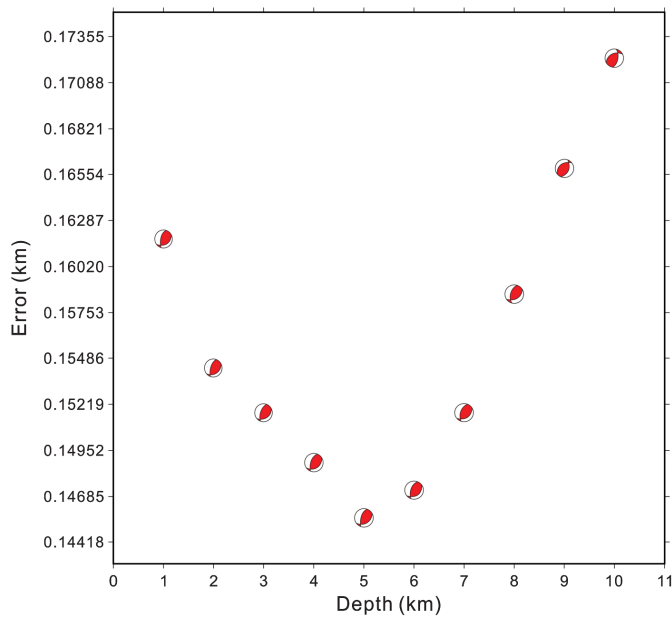


**Figure 2.** The misfit error trade-off with the focal depth for the 8 September 2019  $M_w$  5.2 event.

## Data and Methods

We used seismic reflection profiles that cross the Weiyuan anticline, relocated seismicity, and focal mechanisms to construct a seismotectonic model for the 2019  $M_w$  4.3 and  $M_w$  5.2 earthquakes that occurred in Sichuan, China (Figs. S1–S3, available in the supplemental material to this article). These high-resolution seismic reflection profiles were acquired by PetroChina in 2005 and provided clear images of subsurface faults and horizons in the vicinity of the epicenters. Based on sonic logging data, a regional 3D velocity model (Wang *et al.*, 2016)

was used to convert the seismic reflection profiles from a time domain to a depth domain. Quantitative fault-related fold theory was used to interpret subsurface structures and analyze the kinematic processes. A structural deformation forward modeling application, StructureSolver 4.0, was used to conduct forward modeling simulations (Eichelberger *et al.*, 2017). A 3D structural model of the Weiyuan anticline that included its coseismic fault surfaces, other major fault planes, and related folds was constructed based on seismic interpretation results from stratigraphic and fault picks from the 2D seismic reflection profiles. We used the double-difference relocation method (Waldhauser and Ellsworth, 2000) to relocate the seismic events. For the 2019  $M_w$  5.2 earthquake sequence, we relocated the seismicity by using the crust 1.0 velocity model (Laske *et al.*, 2013). Focal mechanism solutions of the  $M_w$  5.2 earthquake were determined by the cut-and-paste method (Zhu and Helmberger, 1996) (see Figs. 2 and 3 for the location error and waveform fitting information).

## Results

### Basement-involved structural wedge model

We selected three seismic reflection profiles: AA', BB', and CC' (interpreted profiles in Fig. 4, and uninterpreted profiles in Fig. S2) that lie subparallel to the strike of the main fold axis, to show the transverse section features beneath the Weiyuan anticline. Our interpretations show that the structure of the Weiyuan anticline is generally consistent with the basement-involved structural wedge model (Medwedeff, 1992; Shaw *et al.*, 2005; Guzofski *et al.*, 2007; Mount *et al.*, 2011). A structural wedge model contains two connected reverse-thrust fault segments, which typically include either two ramps or one ramp and one detachment that form a wedge-shaped fault block and merge at the tip of the wedge (Shaw *et al.*, 2005). The two faults are connected to the wedge tip and propagate

TABLE 1

**A List of Possible Induced Earthquakes  $M_w > 5$  from 2013 to 2019 in the Shale Gas Blocks of Sichuan Basin (Data from U.S. Geological Survey [USGS] Earthquake Center)**

Time (yyyy/mm/dd hh:mm:ss.ssss)	Longitude (°)	Latitude (°)	Magnitude
2019/09/07 22:42:14.817Z	104.9309	29.5295	$M_w$ 5.0
2019/07/04 02:17:58.120Z	104.8396	28.4885	$M_w$ 5.1
2019/06/22 14:29:56.148Z	104.8105	28.3946	$M_w$ 5.3
2019/06/17 15:36:02.681Z	104.8739	28.4397	$M_w$ 5.1
2019/06/17 14:55:44.876Z	104.9333	28.4056	$M_w$ 5.8
2018/12/16 04:46:09.860Z	105.0128	28.2948	$M_w$ 5.3
2015/02/06 21:01:07.800Z	104.8941	28.3512	$M_b$ 5.0
2013/04/24 22:10:30.700Z	104.956	28.382	$M_b$ 5.3

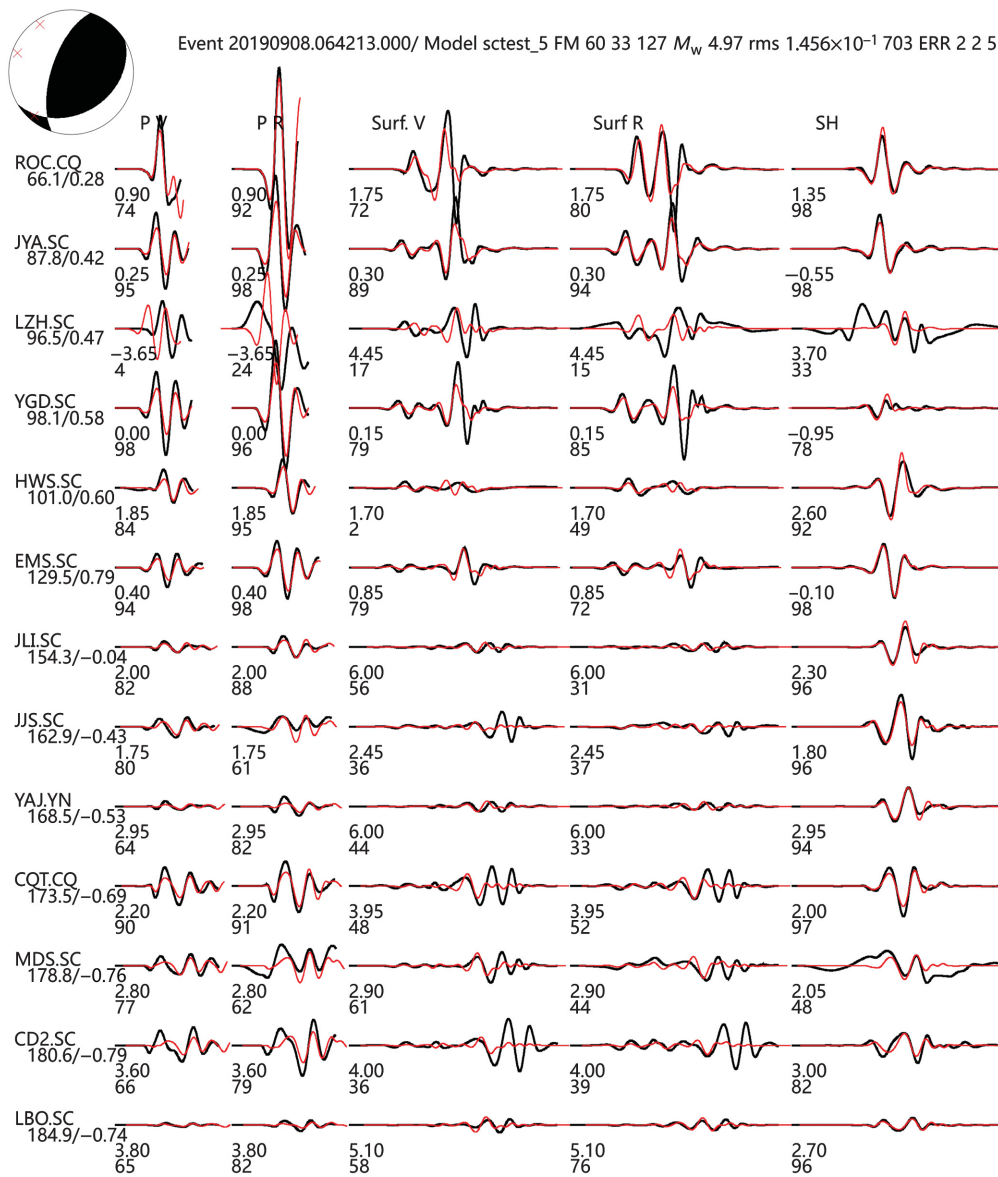


**Figure 3.** The waveform fitting information for the 8 September 2019  $M_w$  5.2 event.

along the detachment to the interior of the foreland basin (Shaw *et al.*, 2005).

The structural wedge model of the Weiyuan anticline includes a western dipping, multibending deep thrust ramp, and three regional detachments, including a Cambrian shale detachment (abbreviated as D1), Silurian shale detachment (abbreviated as D2), and Triassic evaporate detachment (abbreviated as D3), that extend from the regional seismic stratigraphic correlation to the anticline; and back thrusts (BTs; Figs. 4 and 5). The locations of the BTs in section A–A' and B–B' were interpreted based on evidence of direct fault plane reflections or stratigraphic cutoffs in the seismic reflection profiles (Fig. 2). The wedge tip was inferred to be located in the sedimentary cover and the fault slip was

interpreted as having propagated westward along the BTs to offset the stratigraphic layers through Cambrian to Silurian (Fig. 4a,b). In this model, the deep thrust ramp, D1, and the BT comprise structural wedge model, and D2 and D3 were involved in passive folding in the hanging-wall deformation of the wedge model.

### Co-seismic fault models of the $M_w$ 4.2 and $M_w$ 5.2 earthquakes

First, we present the relocated microearthquakes that occurred from January to March 2019 (H. Yang *et al.*, unpublished manuscript, 2020, see [Data and Resources](#); Yang *et al.*, 2020) and in September 2019, shown as yellow and blue dots on the geologic map of the Weiyuan anticline, respectively (Fig. 1b). The focal mechanism solutions of the two mainshocks are illustrated as focal mechanism plots in Figure 1b. We found that most of the aftershocks of the  $M_w$  4.3 and  $M_w$  5.2 mainshocks occurred in two clusters located on the eastern frontal limb of the Weiyuan anticline.

Seismic interpretations show that two tear faults (Ft1 and Ft2) occurred above the D3 and that displaced seismic

reflectors were present within the Triassic Leikoupo and Xujiahe Formations (interpreted profiles in Fig. 5a, and uninterpreted profiles in Fig. S3a). The displacements of Ft1 and Ft2 are 0.3–0.57 and 0.12–0.57 km, respectively (Fig. 6). The mainshock ( $M_w$  4.3) was located near the Ft1 fault plane (Fig. 5a), suggesting that this earthquake was caused by seismic slip along the Ft1 fault. Analysis of the focal mechanism solution shows that the strike of nodal plane 1 was consistent with the fault plane interpreted from the seismic reflection profile (Fig. 5a) (H. Yang *et al.*, unpublished manuscript, 2020, see [Data and Resources](#); Yang *et al.*, 2020). In addition, planar analyses show that the trending of nodal plane 1 from the focal mechanism solution is located  $\sim 24^\circ$  oblique to the surface trace of the northeast–southwest-trending Molin fault (Fig. 1).

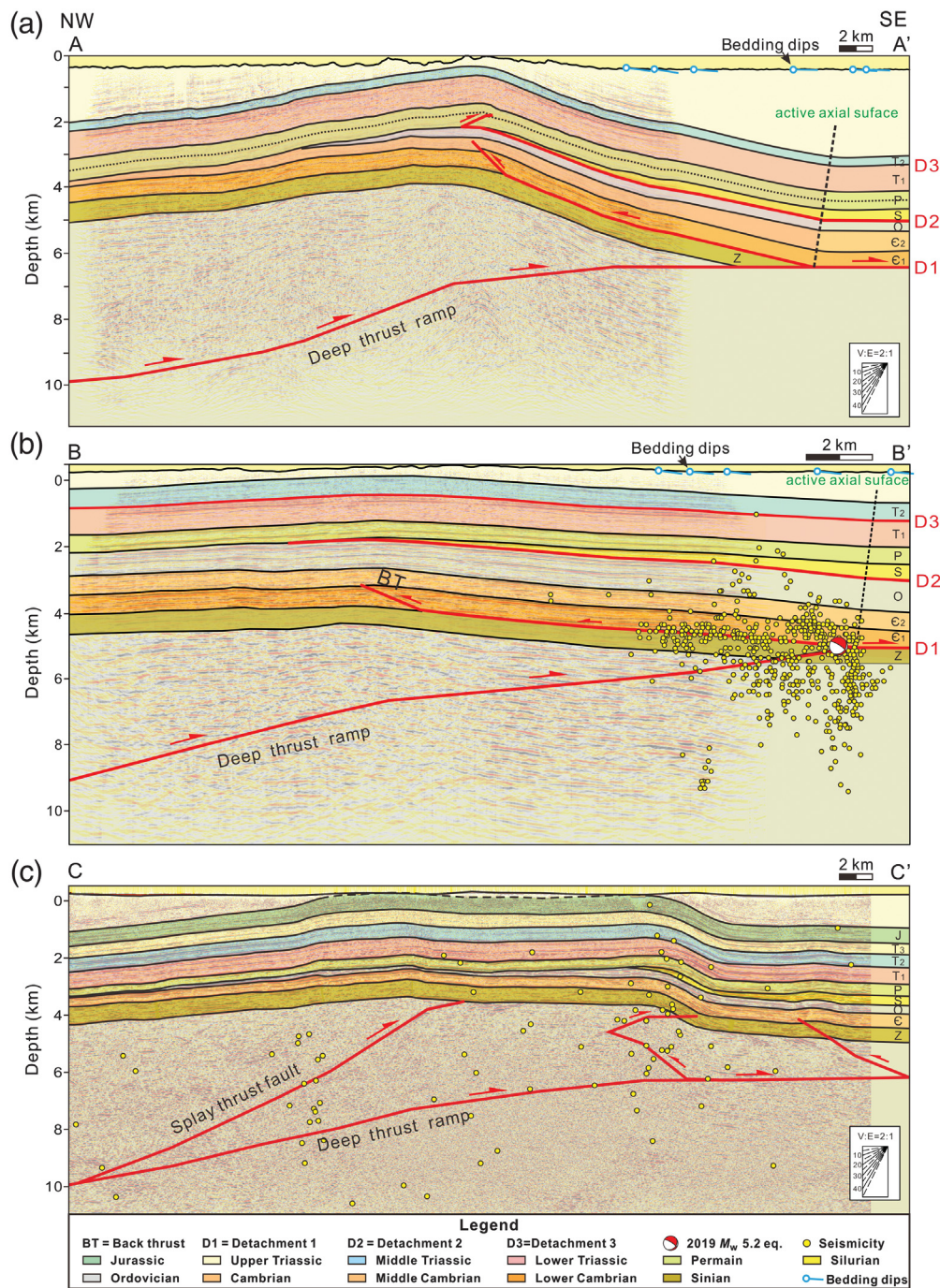


**Figure 4.** Interpreted seismic reflection profiles AA', BB', and CC' images of the (a) representative section of structural wedges beneath the Weiyuan anticline, (b) geologic cross section across the location of the 2019 Weiyuan  $M_w$  5.2 earthquake, and (c) geologic cross section across the southwest edge of the Weiyuan anticline. (Inset) V:E = 2:1 represents that cross sections AA' and CC' are vertically exaggerated (x2), and no vertical exaggeration for section BB'. Yellow spheres in section BB' are aftershocks of the 2019  $M_w$  5.2 Weiyuan earthquake. Yellow spheres in section CC' are hypocenters that were recorded 2013–2016 from (Xin et al., 2018). BT, back thrust; D1, detachment 1, Cambrian shale detachment; D2, detachment 2, Silurian shale detachment; D3, detachment 3, Triassic evaporite sequence detachment; HF, hydraulic fracturing.

In addition, based on geologic mapping and digital elevation model, we found that the Molin fault lies perpendicular to the strike of the Weiyuan anticline and that it forms a distinct

topographic lineament (Ft1 in Fig. 7), which confirms that the Molin fault is a tear fault that formed in the frontal limb of the Weiyuan anticline. This relationship indicates that co-seismic fault slip occurs obliquely along the Ft1 fault, which is consistent with the pattern of oblique tear faulting reported by other studies (Mueller and Talling, 1997).

We also analyzed the structural characteristics of the seismogenic fault for the  $M_w$  5.2 Weiyuan earthquake. Relocated seismicity results indicate that the  $M_w$  5.2 earthquake and many of its aftershocks ruptured the down-dip portion of a gently eastward-dipping back thrust (Fig. 4b), which is consistent with the interpreted BT fault plane derived from the structural wedge model. The focal mechanism solution of the  $M_w$  5.2 earthquake also shows that the co-seismic fault was an eastward dipping thrust fault with a hypocentral depth of 5 km and vertical and horizontal errors of 0.5 and 0.2 km, respectively (Fig. 4b). Seismic interpretation illustrates that the back thrust contains two segments: the up-dip portion is a short (~2 km) and steeply dipping thrust fault (30°), whereas the down-dip portion is a long (~12 km) and gently dipping (10°) detachment fault (Fig. 4b). The down-dip portion of the back thrust is rooted in the Cambrian shale detachment of sedimentary cover and can be extended to connect with the deep basement thrust ramp at a depth of ~5 km (Fig. 4b). Considering the vertical errors in seismic location, these results demonstrate that the mainshock of the  $M_w$  5.2 earthquake ruptured the back thrust and released most of its aftershocks in the back thrust

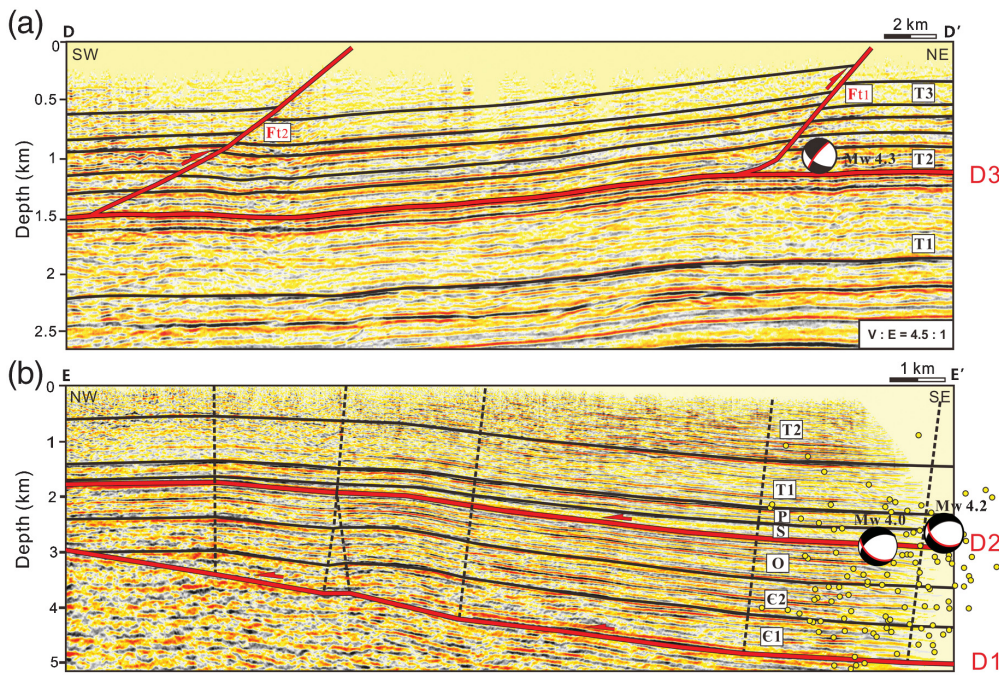


**Figure 5.** (a) Interpreted seismic reflection profile across the epicentral location of the 2019  $M_w$  4.3 earthquake. (b) Interpreted seismic reflection profile across the epicentral location of the two foreshocks of  $M_w$  4.2 and  $M_w$  4.0 earthquakes that occurred before the  $M_w$  4.3 mainshock. Cross sections AA' is vertically exaggerated ( $\times 4.5$ ), and no vertical exaggeration for section BB'. D1, detachment 1, Cambrian shale detachment; D2, detachment 2, Silurian shale detachment; HF, hydraulic fracturing interval. Yellow spheres in section BB' are foreshocks and aftershocks of the 2019  $M_w$  4.3 Weiyuan earthquake sequence.

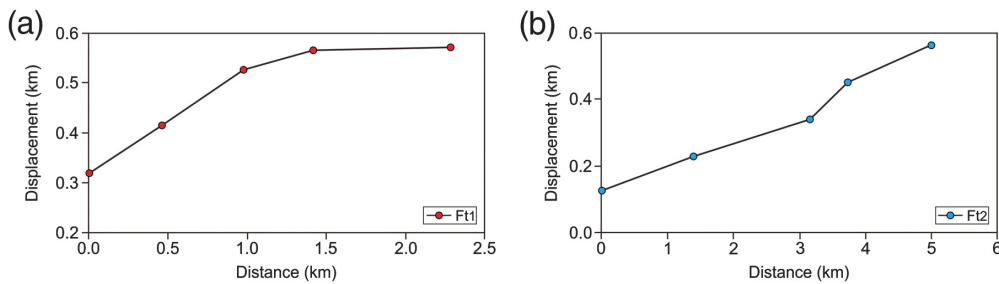


**Figure 6.** (a) The fault displacement–distance relationships of the tear fault, Ft1; (b) the fault displacement–distance relationships of the tear fault, Ft2. Distance, distance along the fault plane; and Displacement, fault displacement

and deep thrust ramp in the vicinity of the structural wedge tip (Fig. 4b).

### Spatiotemporal evolution of seismicity, seismotectonic analyses, and seismic hazard

To investigate the relationships between earthquake activity, fault structure, and HF operations, we analyzed the 25 February  $M_w$  4.3 earthquake sequence (H. Yang *et al.*, unpublished manuscript, 2020, see [Data and Resources](#); Yang *et al.*,

2020) in the Weiyuan anticline. 3D spatial analyses of this earthquake sequence show that stable background seismic swarms at locations S1 and S2 were closely related to the locations of shale gas HF wells (Figs. 1b and 8). We recorded these events according to the time (relative day [RD]) of occurrence and assigned the mainshock, which occurred on 25 February 2019, as day 0 (Fig. 8). The planar views (Fig. 8) show the earthquake events that occurred before the mainshock as a continuous color gradient (blue to green), whereas the events that occurred after 25 February are shown in red (Fig. 8). We also identified two subseismic clusters, S3 and S4, in the vicinity of the Molin fault (the statistics of the sub-seismic clusters are shown in Fig. 9). However, S5 subseismic cluster, which is located to the northeast of the anticline near the epicenter of the September  $M_w$  5.2 earthquake (Fig. 8a), may not represent the aftershocks of the February  $M_w$  4.3 mainshock but rather the microseismic activity caused by HF.

We found that the 25 February 2019 Weiyuan earthquake sequence exhibits properties of a cascading series of foreshocks and aftershocks. The  $M_w$  4.3 mainshock occurred between these two background seismic swarms at a depth of 1 km and is generally consistent with the location of the Ft1 fault plane (Figs. 5 and 8) (H. Yang *et al.*, unpublished manuscript, 2020, see [Data and Resources](#); Yang *et al.*, 2020). However, the mainshock generally lacked aftershocks distributed along the thrust ramp of Ft1. More important, we identified two foreshocks with magnitudes greater than 4.0 that correspond to  $M_w$  4.2 and  $M_w$  4.0 events that occurred on 23 and 25 February, respectively (interpreted profiles in Fig. 5b, and uninterpreted profiles in Fig. S3b). The depths of these two foreshock events

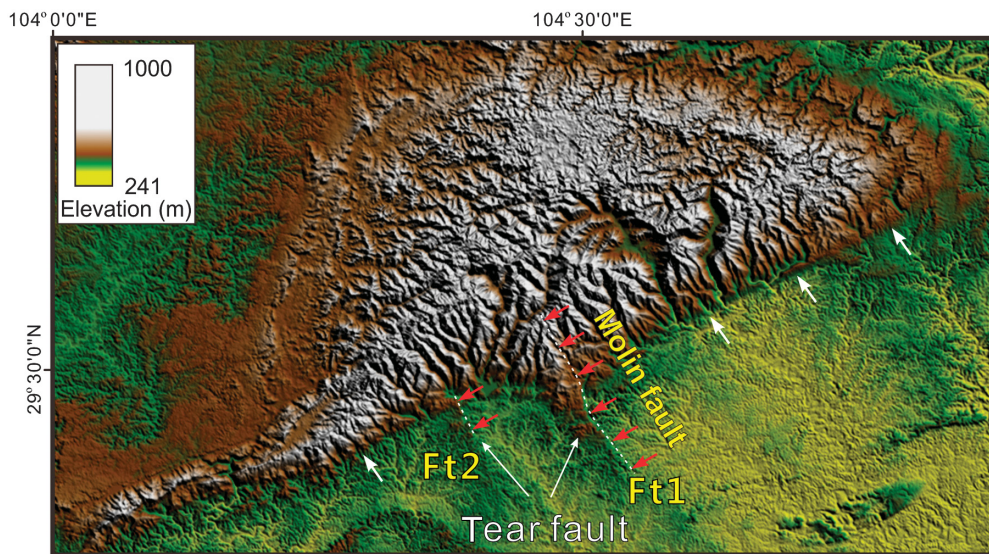


**Figure 7.** Topographic map of the Molin fault in the southeast limb of the Weiyuan anticline and adjacent regions. The surface trace of tear faults Ft1 (Molin fault) and Ft2 are illustrated as red arrows and white dashed lines. The surface trace of the Molin fault is used to constrain the tear fault in the 3D structural model of the Weiyuan anticline.

were  $2.6 \pm 0.5$  and  $2.9 \pm 0.5$  km (H. Yang *et al.*, unpublished manuscript, 2020, see [Data and Resources](#); Yang *et al.*, 2020), which are within the depth range of the Silurian Longmaxi Formation shale that is the target of current HF operations. Combined with the seismic reflection profiles and 3D structural models, our analysis of the focal mechanism solution shows that the two foreshock events occurred on a northeast-trending, eastward-dipping back thrust fault (Fig. 5b). This back thrust is rooted in the Silurian shale formation that is defined as a regional detachment fault in the western Sichuan basin, as demonstrated by the D2 detachment in the structural wedges model (Fig. 4a). The wedge structure model also shows that the D2 detachment was passively involved in deformation during the shortening of the Weiyuan anticline, forming a back thrust that dips gently ( $6^\circ \pm 2^\circ$ ) to the east.

We also analyzed the spatial relationship between the aftershock's distribution of the  $M_w$  5.2 events and fault structures beneath the Weiyuan anticline (Fig. 8b–d). This fault system includes the HF of the Silurian shale detachment fault and the Cambrian shale detachment rooted-back thrust faults. Our results show that seismicity distribution in February was located mainly around the zone of the hydraulically fractured Silurian shale (Fig. 8b,c). We lack seismic monitoring records from March to August 2019. However, the aftershocks from the September  $M_w$  5.2 earthquake were mainly in the proximity of the lower Cambrian shale horizon (Fig. 8b,d), suggesting that this earthquake might have ruptured a detachment-rooted back thrust in the structural wedges beneath the Weiyuan anticline. This spatiotemporal analysis reveals that the  $M_w$  5.2 earthquake occurred  $\sim 2$  km below

the developing Silurian shale formation, which is deeper than the HF zone.

Based on the previous analysis of the mechanism inducing earthquakes, we infer that the Weiyuan anticline may contain the following sources of seismic hazards: (1) hydraulic fractured shale formation; (2) pre-existing faults in the sedimentary cover; and (3) basement involved faults. Specifically, these sources correspond to the following fault systems in the Weiyuan anticline: (1) a tear fault in the shallow sedimentary cover ( $<1.5$ – $2$  km) (Fig. 5a), (2) a detachment fault in Silurian shales at  $2.5$ – $3$  km (Fig. 5b), (3) a back thrust in the deep sedimentary cover ( $4$ – $5$  km)

(Fig. 4a,b), and (4) a seismogenic thrust ramp in the basement ( $>5$  km) (Fig. 4b,c). Therefore, we evaluated the seismic hazard potential of each of the four fault types based on the empirical relationships between fault area and magnitude (Wells and Coppersmith, 1994). The results indicate that the tear fault, Silurian shale back thrust, Cambrian shale back thrust, and the deep thrust ramp in the basement, if completely ruptured, could produce earthquakes of magnitudes 5.9, 6.9, 6.9, and 7.5, respectively (Table 2). We emphasize that the third type of Cambrian back thrust, which can be linked to the deep seismogenic thrust ramp, may represent a relatively significant earthquake source (Fig. 4c).

## Discussion

Recent field studies and numerical modeling have illustrated that earthquakes related to hydraulic fracturing [HF] can occur several kilometers away from the operating well (Holland, 2013; Lei *et al.*, 2017; Schultz *et al.*, 2017; Kozłowska *et al.*, 2018; Schultz and Wang, 2020). For example, in western Canada and southern Sichuan basin, recent earthquake events with  $M_w > 3.0$  showed that the stress changes caused by HF could activate ancient faults beneath a shale formation that extend to a crystalline basement (Bao and Eaton, 2016; Lei *et al.*, 2017). Pressure diffusion caused by injecting fluid into the fault zone that connects to the basement can explain fault reactivation in the basement and the subsequent extensive seismic activity (Galloway *et al.*, 2018; Kolawole *et al.*, 2019). Current industry strategies to mitigate induced earthquakes advocate for the direct injection of fluid into sedimentary cover to avoid activating basal faults. However, for sedimentary

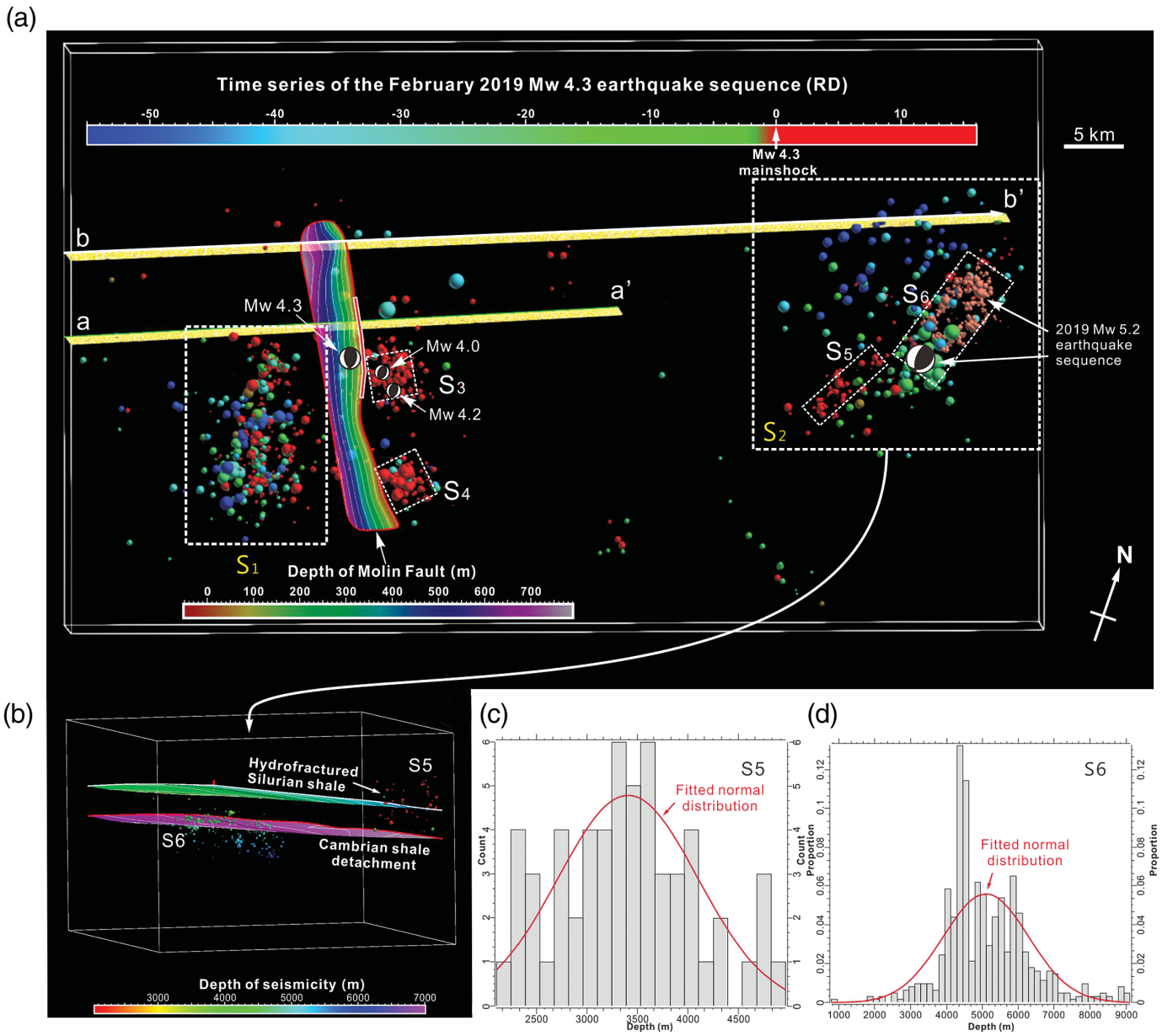


**Figure 8.** (a) Planar view of the 2019  $M_w$  4.2 and  $M_w$  5.2 earthquake sequences and 3D model of the Molin fault and two selected seismic reflection profiles (see Fig. S1 for specific locations). The focal mechanism solutions of two foreshocks  $M_w$  4.2 and  $M_w$  4.0, and the mainshock  $M_w$  4.3 are shown as black-and-white focal mechanism plot. S1, seismic cluster 1; S2, seismic cluster 2; S3, aftershocks of the  $M_w$  4.2 earthquake; S4, aftershocks of the  $M_w$  4.2 earthquake; S5, subseismic cluster; S6, aftershocks of the  $M_w$  5.2 earthquake. (b) 3D model of seismicity distribution and fault system included Silurian shale detachment fault and Cambrian shale back thrust. (c) Microseismic distribution in late February to early March. (d) Depth distribution of the mainshock  $M_w$  5.2 and its aftershocks during 8–12 September.

cover-related induced earthquakes, recent studies based on global cases suggest that fluid injection may induce fault reactivation and produce larger seismic events that are located  $>10$  km from the wellbore (Goebel and Brodsky, 2018). In contrast to injecting water into the underlying basement, injecting fluid into the sedimentary cover promotes pressure and elastic stress on the surrounding sedimentary rock, which then exerts pressure on distal faults. Thus, this type of poroelastic effect that affects the ability of rocks to transfer fluid stresses to solid rocks can produce stronger, more distant earthquakes (Goebel and Brodsky, 2018).

In the Weiyuan Shale gas block, HF within the sedimentary cover may induce the reactivation of different levels of faults through (1) pore-pressure diffusion and/or (2) poroelastic effects. Because of the lack of fluid data, we cannot apply geo-mechanical modeling to directly identify the mechanisms that

induce earthquakes in the Weiyuan block. However, high-resolution seismic reflection profiles can be used to identify the absence of fault connections between HF levels and

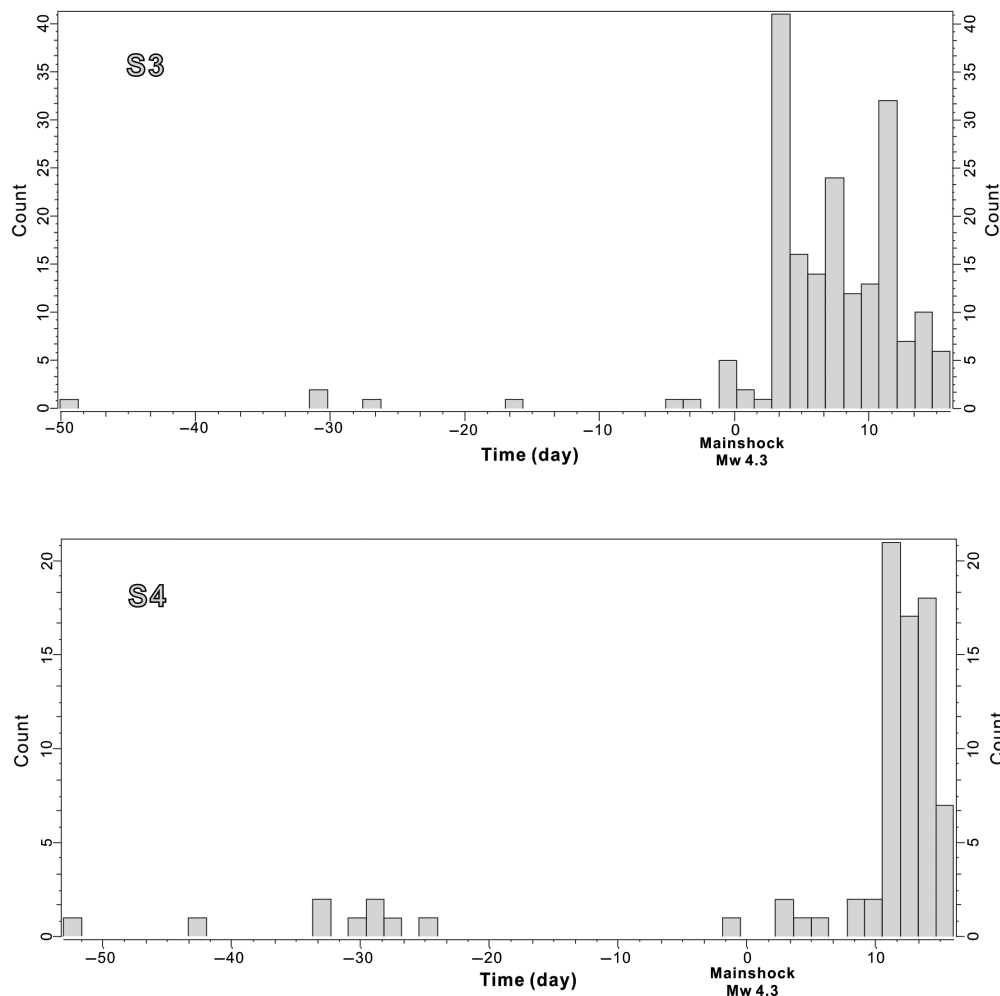


**Figure 9.** The statistics of the sequence of earthquake events that occurred at positions S3 and S4. The locations of S3 and S4 are shown in Figure 8.

co-seismic slip faults, which are essential for the pore-pressure diffusion mechanism. Relocated earthquakes and focal mechanisms demonstrate that the  $M_w$  5.2 earthquake ruptured

**TABLE 2**  
**Possible Earthquakes Scenarios Involving the Faults in the Weiyuan Block, Based on Empirical Relations of Fault Area and Maximum Potential Magnitude**

Fault List	Fault Area (km <sup>2</sup> )	Magnitude ( $M_w$ )
Tear fault (Molin fault)	52.8	5.9
Silurian shale back thrust	800	6.9
Cambrian shale back thrust	750	6.9
Deep thrust ramp	3000	7.5

the back thrust in Cambrian shale, which is located  $\sim 2$  km beneath the HF level in the Silurian shale (Fig. 4b). Seismic reflection profiles reveal no direct fault connection between the two structures. Thus, we infer that the poroelastic mechanism may explain the  $M_w$  5.2 earthquake that occurred on the back thrust in the sedimentary cover. The direct injection of fluids generated from HF of the shale formation promotes fluid pressure diffusion along the Silurian detachment fault, resulting in several foreshocks of  $M_w \sim 4-4.2$ . However, we cannot exclude the potential of the coupled effect of pore-pressure diffusion and poroelastic stresses to induce the two foreshock events. This seismic activity may further induce the reactivation of the 1 km deep tear fault through static stress and/or poroelastic effect, producing the subsequent  $M_w$  4.3 mainshock that occurred on the Molin fault.

## Conclusions

Based on the analyses of seismic reflection profiles, relocated seismicity, focal mechanism solutions, and surface geology, we found that the Weiyuan anticline in the Sichuan basin is underlain by structural wedges and multiple detachment faults. The structural wedge beneath the Weiyuan anticline is composed of a multibending thrust ramp and a back thrust that merges with a Cambrian shale detachment. Based on the temporal and spatial correlations with fracking wells, we reveal that these earthquake events may be caused by hydraulic fracturing through reactivation of pre-existing faults. The 2019  $M_w$  5.2 Weiyuan earthquake sequence ruptured the Cambrian shale back thrust and deep thrust ramp at a depth of  $\sim 4-6$  km, the aftershocks of which were concentrated at the tip of the structural wedge. This seismogenic fault is located  $\sim 2$  km below the fracturing horizon and shows no evidence of a fault connection between these two structures. Therefore, we infer that the poroelastic effect may be the mechanism that induced the 2019  $M_w$  5.2 Weiyuan earthquake. We also found that the 2019  $M_w$  4.3 Rongxian

earthquake ruptured a tear fault perpendicular to the fold axis and can be connected downward to the ~1.75 km deep Triassic detachment fault. The two foreshock events ( $M_w$  4.0 and 4.2) of the  $M_w$  4.3 earthquake ruptured an east-dipping back thrust fault, consistent with the location of the fracturing Silurian shale formation. Therefore, we infer that pore-pressure diffusion may be the mechanism that induces these two foreshocks. However, we cannot exclude the likelihood that coupling effects of pore-pressure diffusion and poroelastic induce these foreshocks.

The Weiyuan anticline is an active structural wedge with frequent seismic activity (Figs. 1 and 4c); hence, the shear stress applied to the deep thrust ramp may approach the fault critical strength. Therefore, fluid injection operations during shale gas production should be monitored to prevent large increases in pore pressure within the fault zone and/or stress changes above the fault plane. Future studies should establish coupled flow-geomechanics simulations to integrate the local geology, seismotectonic models, fluid pressures, and flow rates as a mean of assessing and managing the hazards associated with induced seismicity and/or natural tectonic earthquakes in the Sichuan basin.

## Data and Resources

The relocated seismicity data used in this study can be downloaded from the Open Science Framework (<https://osf.io/6uw97> and <https://osf.io/rbwvg>, last accessed June 2020). Seismic reflection profiles were provided by PetroChina Company and are proprietary. They cannot be released to the public. The supplemental material for this article includes the locations of 2D seismic reflection profiles used to build the subsurface structural model and uninterpreted depth-converted 2D seismic reflection profiles across the southwest portion of the Weiyuan anticline.

## Acknowledgments

This research was jointly supported by National Key R&D Program of China (2018YFC1504104), China National Natural Science Foundation (NSFC) (41702202), Jiangsu Natural Science Foundation (BK20170868), Research Grants Council (RGC) of the Hong Kong Special Administrative Region (HKSAR), China, under the NSFC/RGC Joint Research Scheme (N\_CUHK430/16), and RGC-Germany Joint Research Scheme (G-CUHK408/19). The authors appreciate PetroChina for providing the seismic reflection profiles. The unpublished manuscript by H. Yang, P. Zhou, N. Fang, G. Zhu, W. Xu, and J. Su (2020), "A shallow shock: the deadly February 2019 ML 4.9 earthquake in the Weiyuan shale gas field in Sichuan, China," submitted to *Seismol. Res. Lett.*

## References

Bao, X., and D. W. Eaton (2016). Fault activation by hydraulic fracturing in western Canada, *Science* **354**, no. 6318, 1406–1409.

Burchfiel, B. C., L. H. Royden, R. D. van der Hilst, B. H. Hager, Z. Chen, R. D. King, C. Li, J. Lu, and H. Yao (2008). A geological and geophysical context for the Wenchuan earthquake of 12 May 2008, Sichuan, People's Republic of China, *GSA Today* **18**, no. 7, 5.

Eichelberger, N. W., A. G. Nunns, R. H. Groshong, and A. N. Hughes (2017). Direct estimation of fault trajectory from structural relief, *AAPG Bull.* **101**, no. 5, 635–653.

Ellsworth, W. L. (2013). Injection-induced earthquakes, *Science* **341**, no. 6142, 1225942.

Eyre, T. S., D. W. Eaton, D. I. Garagash, M. Zecevic, M. Venieri, R. Weir, and D. C. Lawton (2019). The role of aseismic slip in hydraulic fracturing-induced seismicity, *Sci. Adv.* **5**, eaav7172.

Frohlich, C. (2012). Two-year survey comparing earthquake activity and injection-well locations in the Barnett Shale, Texas, *Proc. Natl. Acad. Sci. Unit. States Am.* **109**, no. 35, 13934–13938.

Galis, M., J. P. Ampuero, P. M. Mai, and F. Cappa (2017). Induced seismicity provides insight into why earthquake ruptures stop, *Sci. Adv.* **3**, no. 12, eaap7528.

Galloway, E., T. Hauck, H. Corlett, D. Pană, and R. Schultz (2018). Faults and associated karst collapse suggest conduits for fluid flow that influence hydraulic fracturing-induced seismicity, *Proc. Natl. Acad. Sci. Unit. States Am.* **115**, no. 43, E10003–E10012.

Goebel, T. H., and E. E. Brodsky (2018). The spatial footprint of injection wells in a global compilation of induced earthquake sequences, *Science* **361**, no. 6405, 899–904.

Grigoli, F., S. Cesca, A. P. Rinaldi, A. Manconi, J. A. Lopez-Comino, J. F. Clinton, and S. Wiemer (2018). The November 2017 Mw 5.5 Pohang earthquake: A possible case of induced seismicity in South Korea, *Science* **360**, no. 6392, 1003–1006.

Guzowski, C. A., J. H. Shaw, G. Lin, and P. M. Shearer (2007). Seismically active wedge structure beneath the Coalinga anticline, San Joaquin basin, California, *J. Geophys. Res.* **112**, no. B3, doi: [10.1029/2006JB004465](https://doi.org/10.1029/2006JB004465).

Holland, A. A. (2013). Earthquakes triggered by hydraulic fracturing in south-central Oklahoma, *Bull. Seismol. Soc. Am.* **103**, no. 3, 1784–1792.

Hubbard, J., and J. H. Shaw (2009). Uplift of the Longmen Shan and Tibetan plateau, and the 2008 Wenchuan ( $M = 7.9$ ) earthquake, *Nature* **458**, no. 7235, 194.

Hubbard, J., J. H. Shaw, and Y. Klinger (2010). Structural setting of the 2008 Mw 7.9 Wenchuan, China, earthquake structural setting of the 2008  $M_w$  7.9 Wenchuan, China, Earthquake, *Bull. Seismol. Soc. Am.* **100**, no. 5B, 2713–2735.

Jia, D., Y. Li, A. Lin, M. Wang, W. Chen, X. Wu, Z. Ren, Y. Zhao, and L. Luo (2010). Structural model of 2008 Mw 7.9 Wenchuan earthquake in the rejuvenated Longmen Shan thrust belt, China, *Tectonophysics* **491**, nos. 1/4, 174–184.

Jia, D., G. Wei, Z. Chen, B. Li, Q. Zeng, and G. Yang (2006). Longmen Shan fold-thrust belt and its relation to the western Sichuan basin in central China: New insights from hydrocarbon exploration, *AAPG Bull.* **90**, no. 9, 1425–1447.

Jiang, G., X. Qiao, X. Wang, R. Lu, L. Liu, H. Yang, Y. Su, L. Song, B. Wang, and T. Wong (2020). GPS observed horizontal ground extension at the Hutubi (China) underground gas storage facility and its application to geomechanical modeling for induced seismicity, *Earth Planet. Sci. Lett.* **530**, 115943.

Juanes, R., B. Jha, B. H. Hager, J. H. Shaw, A. Plesch, L. Astiz, and C. Frohlich (2016). Were the May 2012 Emilia-Romagna earthquakes induced? A coupled flow-geomechanics modeling assessment, *Geophys. Res. Lett.* **43**, no. 13, 6891–6897.

- Kim, K. H., J. H. Ree, Y. Kim, S. Kim, S. Y. Kang, and W. Seo (2018). Assessing whether the 2017 Mw 5.4 Pohang earthquake in South Korea was an induced event, *Science* **360**, no. 6392, 1007–1009.
- Kolawole, F., C. S. Johnston, C. B. Morgan, J. C. Chang, K. J. Marfurt, D. A. Lockner, Z. Reches, and B. M. Carpenter (2019). The susceptibility of Oklahoma's basement to seismic reactivation, *Nature Geosci.* **12**, no. 10, 839–844.
- Kozłowska, M., M. R. Brudzinski, P. Friberg, R. J. Skoumal, N. D. Baxter, and B. S. Currie (2018). Maturity of nearby faults influences seismic hazard from hydraulic fracturing, *Proc. Natl. Acad. Sci. Unit. States Am.* **115**, no. 8, E1720–E1729.
- Laske, G., G. Masters, Z. Ma, and M. Pasyanos (2013). Update on CRUST1.0—A 1-degree global model of Earth's crust, *Geophysical Research Abstracts*, Vol. 15, 2658.
- Lei, X., D. Huang, J. Su, G. Jiang, X. Wang, H. Wang, X. Guo, and H. Fu (2017). Fault reactivation and earthquakes with magnitudes of up to Mw 4.7 induced by shale-gas hydraulic fracturing in Sichuan basin, China, *Sci. Rept.* **7**, no. 1, 1–12.
- Lei, X., Z. Wang, and J. Su (2019). The December 2018 ML 5.7 and January 2019 ML 5.3 earthquakes in South Sichuan basin induced by shale gas hydraulic fracturing, *Seismol. Res. Lett.* **90**, no. 3, 1099–1110.
- Li, Y., D. Jia, M. Wang, J. H. Shaw, J. He, A. Lin, L. Xiong, and G. Rao (2014). Structural geometry of the source region for the 2013 Mw 6.6 Lushan earthquake: Implication for earthquake hazard assessment along the Longmen Shan, *Earth Planet. Sci. Lett.* **390**, 275–286.
- Medwedeff, D. A. (1992). Growth fault-bend folding at southeast Lost Hills, San Joaquin valley, California, *AAPG Bull.* **73**, no. 1, 54–67.
- Mount, V. S., K. W. Martindale, T. W. Griffith, and J. O. D. Byrd (2011). Basement-involved contractional wedge structural styles: Examples from the Hanna basin, Wyoming, in *Lateral Ramps in the Folded Appalachians and in Overthrust Belts Worldwide: A Fundamental Element of Thrust-belt Architecture*, K. Pohn (Editor), Vol. 2163, U.S. Geologic Survey Bulletin, 2163.
- Mueller, K., and P. Talling (1997). Geomorphic evidence for tear faults accommodating lateral propagation of an active fault-bend fold, Wheeler ridge, California, *J. Struct. Geol.* **19**, nos. 3/4, 397–411.
- Schultz, R., and R. Wang (2020). Newly emerging cases of hydraulic fracturing induced seismicity in the Duvernay East Shale basin, *Tectonophysics* **25**, 228393.
- Schultz, R., R. Wang, Y. J. Gu, K. Haug, and G. Atkinson (2017). A seismological overview of the induced earthquakes in the Duvernay play near Fox Creek, Alberta, *J. Geophys. Res.* **122**, no. 1, 492–505.
- Segall, P., and S. Lu (2015). Injection-induced seismicity: Poroelastic and earthquake nucleation effects, *J. Geophys. Res.* **120**, no. 7, 5082–5103.
- Shaw, J. H., C. D. Connors, and J. Suppe (2005). Seismic interpretation of contractional fault-related folds, *AAPG Stud. Geol.* **53**, 156.
- Skoumal, R. J., R. Ries, M. R. Brudzinski, A. J. Barbour, and B. S. Currie (2018). Earthquakes induced by hydraulic fracturing are pervasive in Oklahoma, *J. Geophys. Res.* **123**, no. 12, 10,918.
- U.S. Geological Survey [USGS] Earthquake Center (2020). National Earthquake Information Center, 27 June 2020, <https://earthquake.usgs.gov/earthquakes/map/> (last accessed June 2020).
- Waldhauser, F., and W. L. Ellsworth (2000). A double-difference earthquake location algorithm: Method and application to the northern Hayward fault, California, *Bull. Seismol. Soc. Am.* **90**, no. 6, 1353–1368.
- Wang, M., J. Hubbard, A. Plesch, J. H. Shaw, and L. Wang (2016). Three-dimensional seismic velocity structure in the Sichuan basin, China, *J. Geophys. Res.* **121**, no. 2, 1007–1022.
- Wang, M., D. Jia, J. H. Shaw, J. Hubbard, A. Plesch, Y. Li, and B. Liu (2014). The 2013 Lushan earthquake: Implications for seismic hazards posed by the Range Front blind thrust in the Sichuan basin, China, *Geology* **42**, no. 10, 915–918.
- Wang, M., and A. Lin (2017). Active thrusting of the Longquan Fault in the central Sichuan basin, China, and the seismotectonic behavior in the Longmen Shan fold-and-thrust belt, *J. Geophys. Res.* **122**, no. 7, 5639–5662.
- Wang, R., Y. J. Gu, R. Schultz, and Y. Chen (2018). Faults and non-double-couple components for induced earthquakes, *Geophys. Res. Lett.* **45**, no. 17, 8966–8975.
- Wei, G., G. Chen, S. Du, L. Zhang, and W. Yang (2008). Petroleum systems of the oldest gas field in China: Neoproterozoic gas pools in the Weiyuan gas field, Sichuan basin, *Marine Petroleum Geol.* **25**, nos. 4/5, 371–386.
- Wells, D. L., and K. J. Coppersmith (1994). New empirical relationships among magnitude, rupture length, rupture width, rupture area, and surface displacement, *Bull. Seismol. Soc. Am.* **84**, no. 4, 974–1002.
- Xin, H., H. Zhang, M. Kang, R. He, L. Gao, and J. Gao (2018). High-resolution lithospheric velocity structure of continental China by double-difference seismic travel-time tomography, *Seismol. Res. Lett.* **90**, no. 1, 229–241.
- Xu, X., X. Wen, G. Yu, G. Chen, Y. Klinger, J. Hubbard, and J. Shaw (2009). Coseismic reverse-and oblique-slip surface faulting generated by the 2008 Mw 7.9 Wenchuan earthquake, China, *Geology* **37**, no. 6, 515–518.
- Yang, H., Y. Liu, M. Wei, J. Zhuang, and S. Zhou (2017). Induced earthquakes in the development of unconventional energy resources, *Sci. China Earth Sci.* **60**, no. 9, 1632–1644, doi: [10.1007/s11430-017-9063-0](https://doi.org/10.1007/s11430-017-9063-0).
- Yang, H., P. Zhou, N. Fang, G. Zhu, W. Xu, J. Su, F. Meng, and R. Chu (2020b). Induced or triggered? The deadly February 2019 Rongxian-Weiyuan ML 4.9 earthquake in the shale gas field in Sichuan, China, paper presented at the 2020 EGU General Assembly, EGU2020-12096, doi: [10.5194/egusphere-egu2020-12096](https://doi.org/10.5194/egusphere-egu2020-12096).
- Zhai, G. Y., Y. F. Wang, Z. Zhou, S. F. Yu, X. L. Chen, and Y. X. Zhang (2018). Exploration and research progress of shale gas in China, *China Geol.* **1**, no. 2, 257–272.
- Zhang, Y., M. Person, J. Rupp, K. Ellett, M. A. Celia, C. W. Gable, B. Bowen, J. Evans, K. Bandilla, P. Mozley *et al.* (2013). Hydrogeologic controls on induced seismicity in crystalline basement rocks due to fluid injection into basal reservoirs, *Groundwater* **51**, no. 4, 525–538.
- Zhu, L., and D. V. Helmberger (1996). Advancement in source estimation techniques using broadband regional seismograms, *Bull. Seismol. Soc. Am.* **86**, no. 5, 1634–1641.

Manuscript received 6 May 2020  
Published online 19 August 2020